Intense narrowband terahertz pulses produced by obliquely colliding laser pulses in helium gas

View Online   Export Citation   CrossMark

Jaeho Lee,[1] (iD) Hyung Seon Song,[1] Dohyun Park,[1] Manoj Kumar,[1] (iD) Bernhard Ersfeld,[2] (iD) Samuel R. Yoffe,[2] (iD) Dino A. Jaroszynski,[2] (iD) and Min Sup Hur[1,a] (iD)

AFFILIATIONS

[1]Ulsan National Institute of Science and Technology, 50 UNIST-gil, Ulju-gun, Ulsan 44919, South Korea
[2]Department of Physics, Scottish Universities Physics Alliance and University of Strathclyde, Glasgow G4 0NG, United Kingdom

[a]Author to whom correspondence should be addressed: mshur@unist.ac.kr

ABSTRACT

A practical configuration for generating narrowband terahertz (THz) pulses based on plasma dipole oscillations (PDOs) is studied using two-dimensional particle-in-cell simulations. In this scheme, two slightly detuned laser pulses collide obliquely in a helium gas. Plasma strips are generated along the paths of the laser pulses by field ionization. The PDO created in the overlap region of the two laser pulses emits a THz pulse with a peak electric field strength of a few gigavolt per meter. An energy conversion efficiency of 0.542×10^{-3} is achieved for laser pulse intensities $4.82 \times 10^{16} \, \mathrm{W/cm^2}$, a spot radii of $5 \, \mu m$, and a collision angle of $10.8°$. A force balance model is extended for the obliquely colliding configuration of the pulses. As the complications, such as generating plasmas separately or aligning the beams with preformed plasma, are eliminated from our new configuration, this makes a future experimental study of PDO more straightforward.

Published under an exclusive license by AIP Publishing. https://doi.org/10.1063/5.0142159

I. INTRODUCTION

Powerful terahertz (THz) radiation sources have recently been proposed for use in applications, such as THz imaging,[1] detection of cancer cells,[2] pump-probe experiments,[3] and terahertz electron acceleration.[4] However, currently available THz sources have both advantages and limitations. Semiconductor oscillators are stable and compact, but because of the junction transit time of carriers, the output frequency range is restricted to subterahertz (200 GHz–1 THz).[5] Quantum cascade lasers (QCLs) can provide continuous-wave (cw) THz radiation in the few-THz range[6] (1–4.4 THz), but their output power is just tens of milliwatts, which is not suitable for high-peak power applications. Recently, lithium niobate crystals have been found to be very efficient sources of tunable THz radiation.[7] However, solid-state systems are generally prone to material damage by high-intensity driving lasers, which limit their scaling to high-power THz.

Laser–plasma interactions can be the basis for alternative high-power THz sources because plasma is already in a broken-down state and not susceptible to material damage. Numerous ideas have been explored; some of which utilize plasma as a source of charge carriers to generate strong radiating currents, while others utilize the plasma waves as radiating antennae. Two-color THz[8] or coherent transition radiation (CTR)[9] fall into the first category, while the Cherenkov wake,[10] mode conversion,[11] two-plasmon merger,[12–14] and the superluminal wakefield scheme in density gradient of a plasma[15] correspond to the second category. Roughly, broadband THz radiation is generated from the first kind, while relatively narrowband pulses are produced from the second. These mechanisms have a common advantage in that there are no practical limitations to increase the power of driving lasers, and, in principle, arbitrarily high-power THz waves can be generated. In systems where the plasma oscillation is used as a source of THz emission, the low conversion efficiency of the plasma wave to the THz is generally of concern. The low efficiency originates, partially, from low coupling of the two waves (plasma and THz waves) as their phase velocities, i.e. (ω, k), vectors do not match exactly.

We previously proposed generating a local ensemble or bunch of electrons that perform plasma oscillations, namely, plasma dipole oscillations (PDOs).[16] In principle, all the electrostatic energy of PDOs can be converted to THz emission, leading to a high coupling efficiency. Furthermore, the monochromatic emission spectrum from PDO is potentially beneficial to applications, which require narrow bandwidth THz radiation.[17–21] The PDO-THz radiator is one of the few sources that can generate narrowband, but simultaneously high-power THz radiation from laser–plasma systems. THz free-electron lasers (FELs) are another class of sources that share similar characteristics but are huge and expensive facilities, which limit their accessibility for various applications.[22,23]

In our previous study,[16] the PDO is generated by two short ($\sim$30 fs) laser pulses colliding head-on in a strip of pre-formed plasma inserted along the path of the laser pulses. The width of the plasma strip is made comparable to the pulse spot diameter to minimize shielding of THz emission by the ambient plasma. However, such configurations have several drawbacks from an experimental point of view: a narrow plasma strip cannot be readily produced and aligning two laser pulse foci and ensuring exact head-on collision in a narrow plasma strip is challenging [Fig. 1(a)]. We show that these issues can be easily solved by generating the plasma strip using the driving pulses themselves via field ionization of neutral gas [Fig. 1(b)]. As the plasma strip is always localized to the laser pulse trajectories, we obtain the freedom to change the collision angle of the pulses at will (i.e., the pulses do not need to propagate anti-parallel along a straight plasma strip); laser alignment is considerably less restrictive. Furthermore, as discussed in our previous study,[16] oblique collision of the driving pulses can potentially have the advantage of increasing the conversion efficiency. In this paper, we present simulation studies showing that the THz radiation can be generated well from ionized plasmas as well as from pre-formed plasma,[16] especially when the driving pulses collide obliquely. Helium (He) has been used as the background neutral gas. From two-dimensional (2D) particle-in-cell (PIC) simulations, we obtained conversion efficiencies of order 10^{-3} and electric field strength of several gigavolt per meter. Simulation results in this paper imply that the PDO-THz can be efficiently generated even under such experiment-friendly conditions, preserving the high efficiency obtained from head-on collision of the pulses in a pre-formed plasma strip. In addition, the efficiency is found to be insensitive to the collision angle of the driving pulses.

The paper is organized as follows. In Sec. II, the force balance model for PDO generation for oblique collision is presented. In Sec. III, the simulation setup using field ionization model are described. Simulation results are presented in Sec. IV. Conclusions are given in Sec. V.
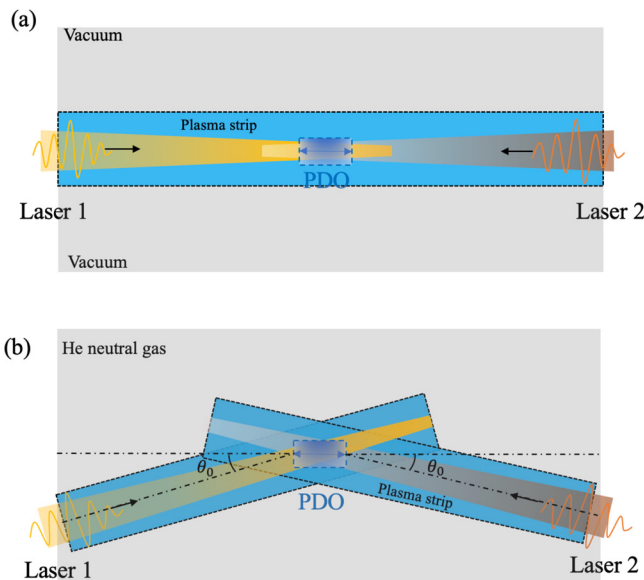

FIG. 1. Illustration of (a) generation of PDO in pre-ionized plasma strip and (b) production of PDO by field-ionization of He gas.

II. THEORETICAL MODEL FOR GENERATION OF PDO

When two slightly detuned laser pulses collide in plasma, electrons are trapped and dragged by the train of beat ponderomotive (PM) potential of the pulses. The trapped electrons move in unison with the phase velocity of the beat wave and are displaced until the ponderomotive force is balanced by electrostatic restoring force of ions. After the laser pulses have passed, the displaced bunch of electrons is released and oscillates at the plasma frequency. We call such a local electron bunch that oscillates in-phase, the plasma dipole oscillator (PDO). The PDO produces a coherent radiation burst with narrow bandwidth centered at the plasma frequency. The theoretical model for the production of a PDO is described in our previous study.[16] Here, we present a slightly modified theory for obliquely colliding laser pulses with angle θ_0. The ponderomotive force for oblique angle is given by

$$f_{pm} = -mc\omega \frac{a^2}{\gamma} \cos\theta_0 \cos 2\theta_0 \left(\frac{1}{2} e^{2ik\cos\theta_0 x - i\Delta\omega t} + c.c. \right), \quad (1)$$

where $\Delta\omega = |\omega_1 - \omega_2|$; $2k = k_1 + k_2$; and m, c, and $\omega_{1,2}$ are the electron mass, speed of light, and the angular frequencies of the laser pulses, respectively. The normalized amplitude of the driving laser field, a, are given by a Gaussian profile,

$$a = a_0 \exp\left[-\frac{(t - t_w)^2}{\tau^2} \right],$$

where t_w and τ are wave-breaking time and pulse duration, respectively, and a_0 is the peak value of the normalized electric field strength defined by $a_0 = eE_0/mc\omega$. Note that the time is arranged so that the wave-breaking occurs at $t = 0$. The cycle-averaged Lorentz factor $\overline{\gamma} = \sqrt{1 + \overline{a^2}} \simeq 1$ for non-relativistic laser pulses ($a_0 \ll 1$). The equation of motion for electrons driven by this ponderomotive force is

$$\frac{\partial^2 \delta x}{\partial t^2} + \omega_p^2 \delta x = -c\omega a^2 \cos\theta_0 \cos 2\theta_0 \left(\frac{1}{2} e^{2ik\cos\theta_0 x - i\Delta\omega t} + c.c \right), \quad (2)$$

where δx is the displacement of an electron fluid element, which can be written as $\delta x = \frac{1}{2}\hat{x}(t) e^{2ik\cos\theta_0 x - i\Delta\omega t} + c.c.$ The equation for the amplitude $\hat{x}$ is then

$$\frac{\partial^2 \hat{x}}{\partial t^2} + \omega_p^2 \hat{x} = -c\omega a^2 \cos\theta_0 \cos 2\theta_0. \quad (3)$$

The amplitude grows until it reaches the wave-breaking limit,[24] given by $\hat{x} \geq 1/k_b$, where $k_b = 2k\cos\theta_0$. The modified condition for wave-breaking is, therefore,

$$\frac{8}{\omega^2 \tau^2 a_0^2} \simeq \frac{e^{-2\xi^2}}{\xi^2 + \omega_p^2 \tau^2/16} \cos^2\theta_0 \cos 2\theta_0, \quad (4)$$

where $\xi \equiv t_w/\tau$, i.e., the time taken to reach the wave-breaking limit, t_w, is normalized by the pulse duration τ. When wave-breaking occurs, electrons are trapped in the PM potential and are dragged with its phase velocity,

$$v_{\phi x} = \frac{\Delta\omega}{2k\cos\theta_0}. \quad (5)$$

With this phase velocity, the electrostatic restoring force increases linearly over time

$$E_{peak} = \alpha \frac{en_0}{\epsilon_0} v_{\phi x} t, \qquad (6)$$

where α is the fraction of trapped electrons. When the ponderomotive force is balanced by the restoring force at $t = t_{rel}$, the maximum dipole field is determined,

$$\frac{eE_{peak}}{mc\omega} = \zeta \frac{a_0^2}{\sqrt{1 + a_0^2/2}} \cos^3\theta_0 \exp\left[-\frac{2(t_{rel} - t_w)^2}{\tau^2}\right]. \qquad (7)$$

Here, ζ is due to the ensemble average of PM forces, which has been confirmed by one-dimensional (1D) PIC simulation to be $\zeta \simeq 0.3$.[16] Note that Eq. (7) has a dependence on θ_0 via the cosine term and t_w, which is obtained from Eq. (4).

III. SIMULATION SETUP

For 2D PIC simulation, we used our in-house code, cplPIC, which has been verified for numerous applications of laser–plasmas.[25–29] The cplPIC code employs the standard Yee-mesh-based field solver,[30] Villasenor–Buneman charge-conserving scheme for current calculation,[31] and Boris mover for particle motion.[32] For field ionization of neutral particles by the laser field, we used the barrier-suppression ionization (BSI) model[33] for electric field larger than the critical field $E(t) > E_{crit}$ and ADK (Ammosov–Delone–Krainov) tunneling ionization model,[34] otherwise . The critical electric field is given by[35]

$$E_{crit} = \left(\sqrt{2} - 1\right)|\xi_i|^{3/2}, \qquad (8)$$

where ξ_i is the ionization energy of the unperturbed electron ground state. The ionization rate from the ADK formula adapted for laser–plasma interaction[35] for He gas is given by

$$W_{He}[s^{-1}] \approx \frac{7.42 \times 10^{18}}{E^{0.492}[GV/m]} \times \exp\left(-\frac{828.26}{E[GV/m]}\right). \qquad (9)$$

Note that the ADK model is determined by numerical solution of the time-dependent nonlinear Schrödinger equation.[36] The ionization rate for He → He$^+$ is shown in Eq. (9), and we also take the same formula into account for He$^+$ → He^{++}.

IV. SIMULATION RESULTS

Figure 2(a) represents the magnetic field (B_z) of the PDO-radiation. The simulation parameters are as follows. The dimension of the simulation domain is $200 \times 200\ \mu m^2$ on an x–y plane. Along the third dimension (z), physical quantities (e.g., B_z) are uniform. The mesh size in each direction is $\Delta x = 5 \times 10^{-8}$ and $\Delta y = 1 \times 10^{-7}$ m, respectively, and the simulation time step is $\Delta t = 1.4 \times 10^{-16}$ s, satisfying the Courant condition. Two linear-polarized (in z direction) Gaussian ($\sim e^{-t^2/\tau^2} e^{-r^2/\sigma^2}$) laser pulses are launched from left and right boundaries of the domain at incident angle $21.8°$ to the horizontal line and collide at the center of the domain ($x = 100$ and $y = 100\ \mu m$). The normalized peak amplitude of the laser pulses, $a_0 = eE_0\lambda_s/(2\pi mc^2) = 0.15$, where e and m are electron unit charge and mass, c is the speed of light, and λ_s is the scale length that is set to $0.8\ \mu m$ in our simulations. Corresponding laser intensity is 4.82×10^{16} W/cm^2. The wavelengths of the laser pulses are $\lambda_1 = 0.8$ (from left boundary) and $\lambda_2 = 0.74\ \mu m$ (from right boundary), respectively. The pulse duration and focal spot radius are set to $\tau = 30$ fs and $\sigma = 5\ \mu m$, respectively. The simulation domain is filled uniformly with neutral helium (He) particles. The He gas density is set to $n_0 = 1.24 \times 10^{24}$ m^{-3} with 10 simulation particles per cell.

To measure the temporally evolving fields of PDO and the associated radiation in He gas, several virtual probes are placed in the simulation domain. The central dipole field, measured at probe 1 (100 μm, 100 μm), grows to approximately (-8 GV/m) during the overlap of laser pulses and commences the plasma oscillation subsequently. Probe 2 and probe 3 are located 2 μm away longitudinally from the central probe 1 and demonstrate how long the locked phase between dipole electrons lasts. It is observed that beyond t = 3.5 ps, the
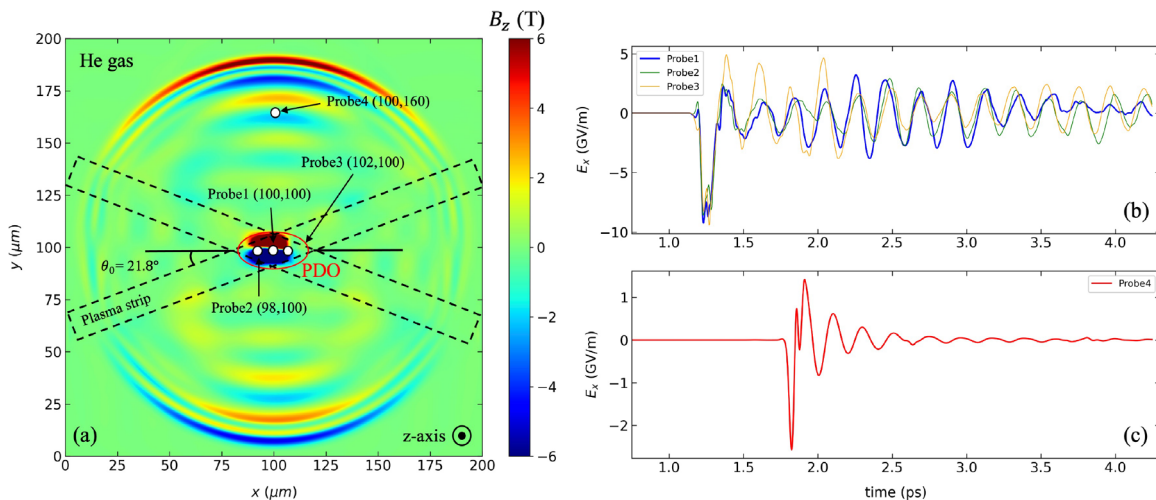
FIG. 2. (a) Magnetic field (B_z) of PDO-radiation at t = 2.12 ps. The laser pulses are incident obliquely with $21.8°$ to the horizontal. High-intensity pulses cause field ionization and create two plasma strips. The small white circles at the center represent the position of virtual probes. The concentric circles, indicating the direction out of the page, represent the z axis. (b) Longitudinal electric field (E_x) obtained from the three different virtual probes; probe 1 is located at the center of the PDO (100 and 100 μm) and probes 2 and 3 at the left and right sides of probe 1 with 2 μm gap. (c) Radiation field (E_x) obtained from probe 4 that is located at neutral He gas, at (100 and 160 μm).

off-central phases are considerably different to the central ones. However, the radiation field E_x [Fig. 2(c)] measured at probe 4 (100 and 160 μm), i.e., non-plasma side, shows that the radiation field decays much faster than that. The long-lasting (lasting over the emission decay) oscillation of the electric field at the dipole center shown in Fig. 2(b) is believed to be wakefield, rather than a dipole oscillation.

The progress of ionization procedure and the plasma electron density near the PDO after the pulse collision is presented in Fig. 3. A density modulation with the beat wavelength and turbulent structure (indicating the wave-breaking) are observed in Fig. 3(a). Figure 3(b) represents the average density in a window around the PDO, i.e., $x = (87–112 \mu m)$, $y = (92–106.5 \mu m)$. With the field strength of the laser pulses, the electrons of neutral helium atoms are stripped off almost instantaneously. The resultant electron density is twice the initial helium density. The power spectra of the electron oscillation at the PDO center and the radiation show monochromatic peaks exactly at the plasma frequency $f_{pe} \approx 14.3$ THz [black dashed line in Fig. 3(c)]. The results described above, i.e., GV/m field strength, narrow spectrum around the plasma frequency, high conversion efficiency of order 10^{-3} (which will be shown later), all indicate that oblique pulse collision in field-ionized plasma can generate THz pulses with similar

efficiency to a head-on collision of the pulses in a pre-formed plasma strip. This result is a useful guide to experiments and relaxes the technical challenges, such as exact head-on collision, generation of a narrow plasma strip, and pulse injection into it, while preserving the high efficiency and strong THz yield found in our previous study.[16]

## A. Parametric study: Effects of detuning, angle, and pulse strength

We examined the effects of various parameters $(\beta_\phi, a_0, \theta_0)$ on generation of PDO and radiation. Here, the velocity of the beat wave of colliding pulses is given by $\beta_\phi = \Delta\omega/(2ck) = v_\phi/c$, i.e., controlled by detuning of the pulse frequencies. In Figs. 4(a)–4(c), the peak electric field at the dipole center, E_{peak}, is measured by varying the laser pulse amplitude a_0, beat velocity β_ϕ, and pulse collision angle θ_0. The theoretical scaling obtained from Eq. (7) predicts well E_{peak}(blue squares) as a function of either a_0 or β_ϕ [Figs. 4(a) and 4(b)]. We find that the angle dependence is weak [Fig. 4(c)]. The red squares in Figs. 4(a)–4(c) represent the electric field of the emitted radiation measured at a distance, from probe 4. The reduction in the field strength is just by the typical $1/\sqrt{r}$ decay of 2D dipole radiation.
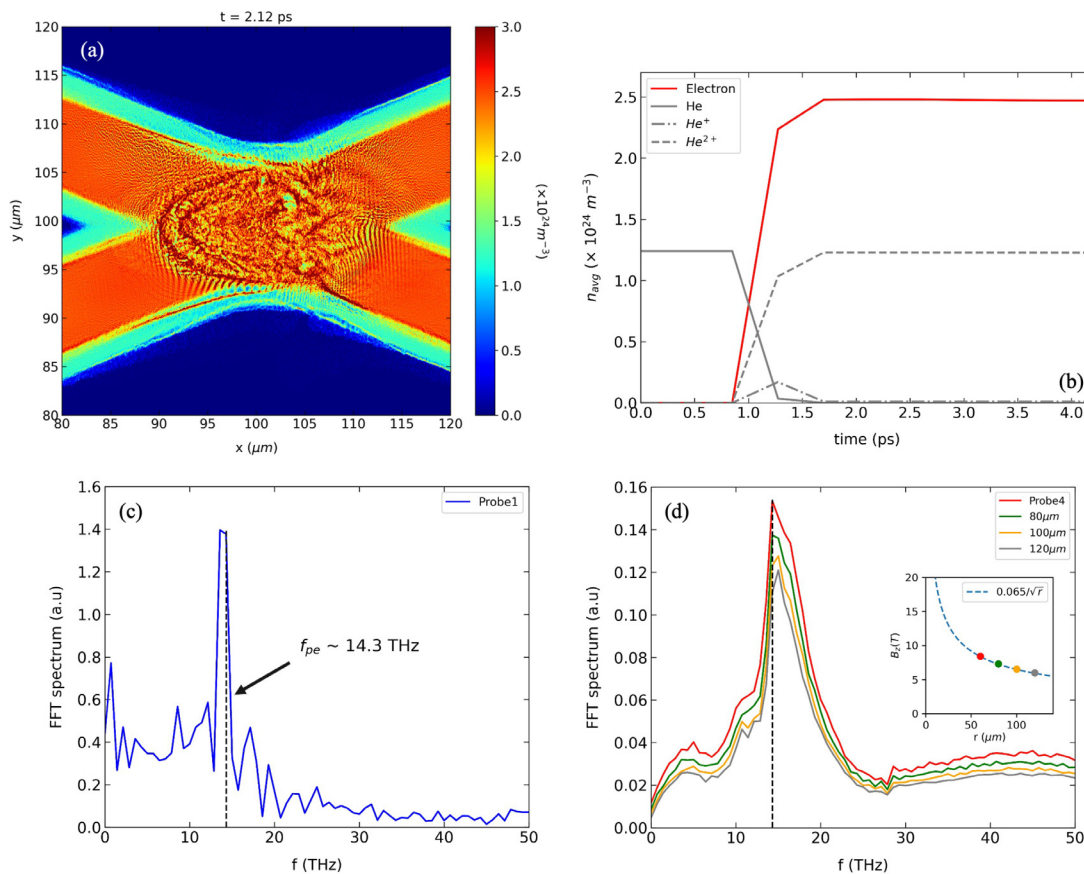
FIG. 3. (a) Electron density (n_e) near the PDO center at t = 2.12 ps. (b) Evolution of averaged electrons, helium ions, and neutral helium density around the PDO. (c) FFT of x directional electric field (E_x) that is obtained from probe 1 in Fig. 2(b). The dashed line shows the expected plasma frequency f_{pe} = 14.3 THz. (d) FFT spectra of E_x obtained from different positions in the far-field radiation zone; red (60 μm), green (80 μm), yellow (100 μm), and gray (120 μm) from the dipole center along the y direction, respectively. The inset is the radiation peak amplitude of B_z vs distance from the dipole center. The dash line (sky-blue) is a fitting curve, 0.065/$\sqrt{r}$.
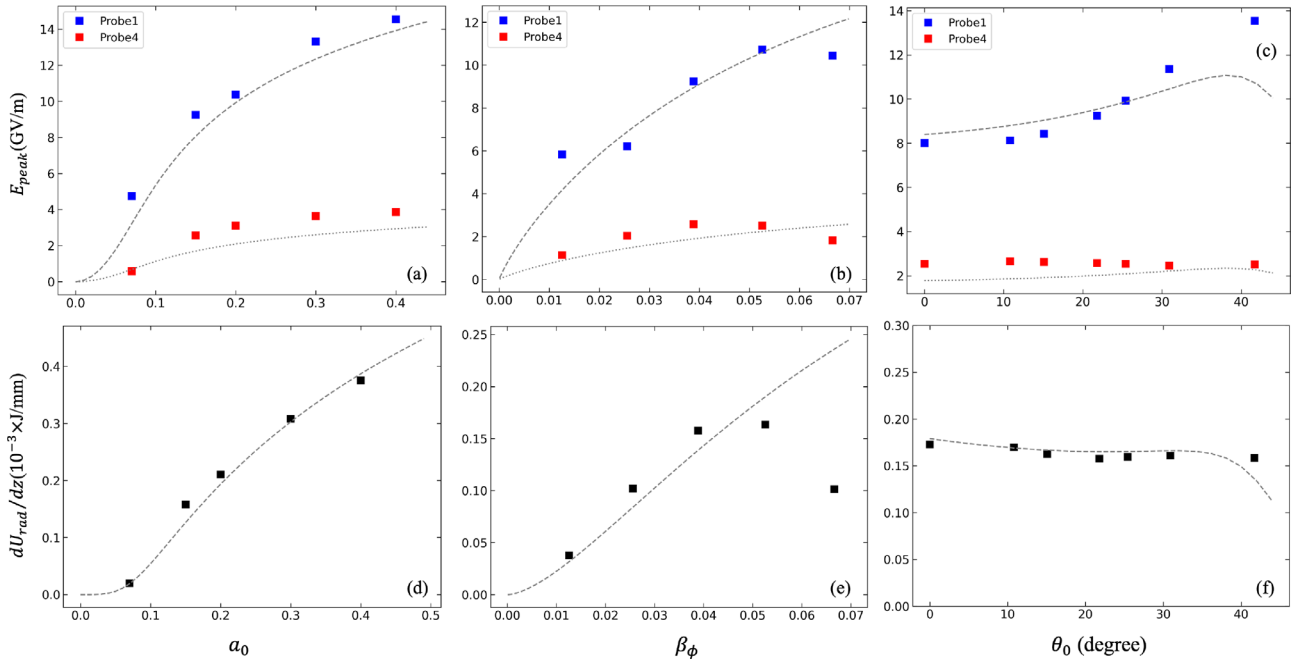
FIG. 4. The peak electric field E_{peak} and radiation energy per unit z directional length dU_{rad}/dz for the change in various parameters (β_ϕ, a_0, and θ_0). For E_{peak}, E_x is measured at probe 1 (blue) and probe 4 (red) corresponding to the placements in Figs. 2(b) and 2(c). The gray dotted and dashed lines represent the theoretical curves obtained from Eq. (7). Theoretical curve fits the simulation data when R = (a) 0.9, (b) 1.0, (c) 0.78–1.0, (d) and (e) 1.0, and (f) 0.99 and $\alpha = 0.83$ and (c–f) $\alpha = 0.7$–1.0.

To calculate the total radiation energy of PDO, we used an array of virtual probes along the horizontal line at $y = +160\,\mu m$ with the $10\,\mu m$ intervals. The total energy radiated per unit lateral length (z) of THz radiation passing through the lines can be calculated as follows:

$$\frac{dU_{rad}}{dz} = \iint \frac{1}{\mu_0} B_z^2\, c\, dt\, dx \simeq \Delta x \sum_i \left[\int \frac{1}{\mu_0} B_z^2 c\, dt \right]_i, \quad (10)$$

where Δx is the interval between the probes and i is the probe index. The time integration is calculated numerically for data obtained from each probe. For a theoretical prediction of the radiation energy, we calculate the total field energy over the dipole region accumulated during the pulse overlap using Eq. (11), with a phenomenological R factor that is the fraction of initial dipole energy converted to radiation energy. We also use another phenomenological factor α, which represents the fraction of trapped electrons. For head-on collision ($\theta_0 = 0$) of the pulses, the PM potential train traps almost all the background electrons ($\alpha \sim 1$), but for oblique collisions of the pulses ($\theta_0 > 0$), the longitudinal component of the PM force is lower than for head-on collision. Thus, we found a lower value of $\alpha = 0.83$ fits best for most of the cases. The total radiation energy vs a_0 is shown in Fig. 4(d), which demonstrates that the radiation energy scales with increasing a_0,

$$\frac{dU_{rad}}{dz} \simeq R\frac{dU_{di}}{dz} = R \iint \epsilon_0 E_{peak}^2(t)\, dx\, dy. \quad (11)$$

Figure 4(e) shows the total radiation energy for varying β_ϕ. Saturation of dU_{rad}/dz for large β_ϕ can be explained by the factor neglected in the theory; for a large β_ϕ, the wave-breaking threshold increases, and the trapped fraction can be reduced. Figure 4(f) shows that the

radiation energy of the PDO, both from theory and simulations, is weakly dependent on the angle (θ_0) of pulse collision. Such insensitivity to the angle can be an advantage for an experimental setup of the system.

Note that in calculation of Eq. (11), we multiply the dipole area to the field square. For calculation of dipole area, in Fig. 5, we compare the measured dipole length with the theoretical estimate, given by
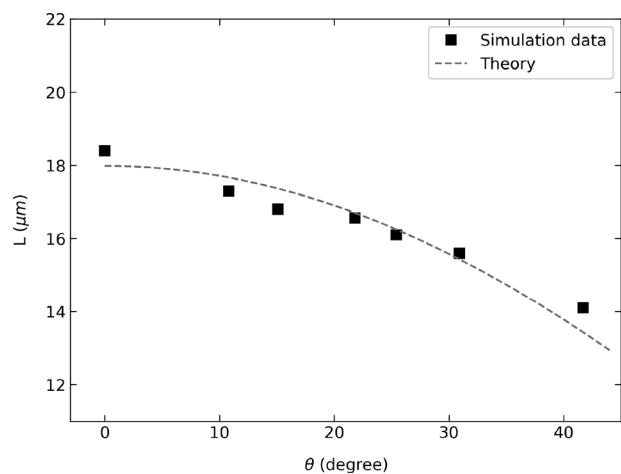
FIG. 5. Dipole length vs collision angle of two laser pulses. The filled squares represent the dipole length measured from the simulations. The gray dashed line is the theoretical curve from Eq. (12).
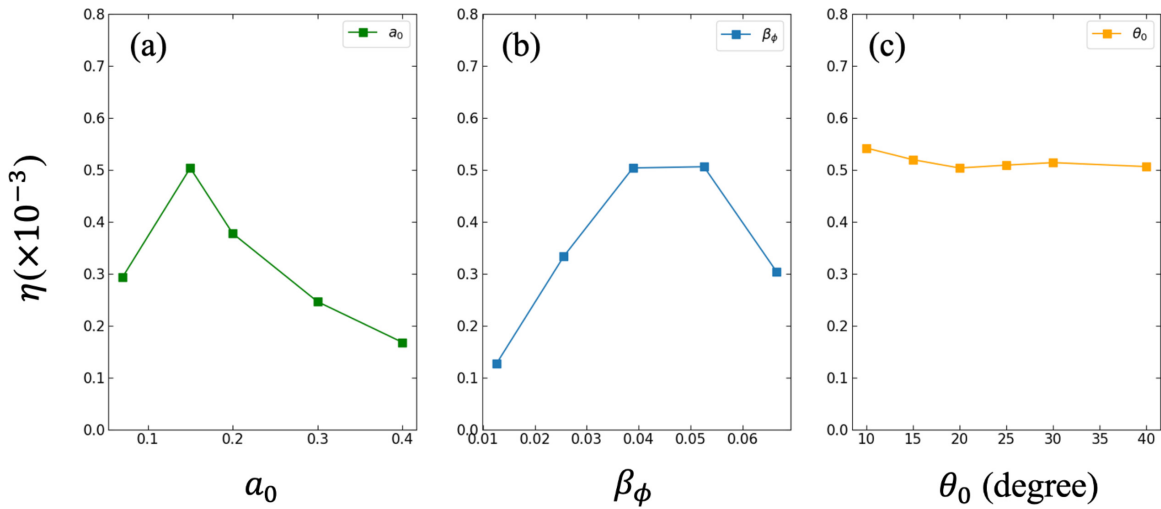
FIG. 6. Energy conversion efficiency (η) vs (a) a_0, (b) β_ϕ, and (c) θ_0.

$$L = 2c\tau \cos\theta_0, \quad (12)$$

where θ_0 is the collision angle of the two laser pulses, τ is the pulse duration, and L is the dipole length. Obviously, the collision angle is the dominating factor determining the dipole length. Figure 5 shows that Eq. (12) agrees well with the simulation data.

One advantage of colliding laser pulses with large angles is that the length of the dipole can be determined by the collision angle of the pulses rather than by the duration of the pulses (when the pulses collide at a no angle, dipole length is determined by pulse duration only $\sim 2c\,\tau$). As the constraint that the pulse length should be kept below the THz wavelength λ_p can be removed, long but weak laser pulses can be used instead of short strong pulses to obtain similar amplitudes of dipole oscillation. This feature can be useful in reducing the cost of the system and, furthermore, increasing the efficiency of laser-to-THz conversion.[16]

B. Energy conversion efficiency

We have calculated the conversion efficiency of driving pulse energy to the PDO radiation energy

$$\eta = \frac{U_{rad}}{U_{laser_1} + U_{laser_2}}, \quad (13)$$

where the denominator represents the energy of the two laser pulses. The total radiation energy has been calculated using Eq. (10). The best efficiency obtained is 0.542×10^{-3} for $a_0 = 0.15$, $\beta_\phi = 0.0389$, and $\theta_0 = 10.8°$. This is a fairly high efficiency, comparable to efficiency $(1.5 \sim 2.2 \times 10^{-3})$ using THz pulse generation in strong magnetized plasma.[37] We expect that it can be increased considerably by optimizing the pulse shape and duration, as suggested in Ref. 16. The efficiency vs β_ϕ [Fig. 6(b)] has a similar tendency to dU_{rad}/dz vs β_ϕ [Fig. 4(e)], which decreases for large β_ϕ. The efficiency peaks at $a_0 \simeq 0.15$ and decreases [Fig. 6(a)]. Since U_{rad} has a very weak angle-dependence [Fig. 4(f)], so does the efficiency [Fig. 6(c)].

V. CONCLUSION

We have examined the feasibility of generation of THz pulses by obliquely colliding two laser pulses in helium gas. The mechanism of THz emission is generating the plasma dipole oscillation (PDO) in a field-ionized plasma. From 2D PIC simulations with the field-ionization based on ADK model, it was demonstrated that plasma strips are created by field ionization, trailing the laser pulses. A PDO is generated in the overlap region of the field-ionizing plasma strips, which results in the emission of strong THz pulses. This result indicates that a strong, *narrowband* THz wave can be generated from a simple, experiment-friendly system of laser–gas interaction, without pre-created plasma. We note that previously, only *broadband* THz pulses have been generated from similarly simple laser-gas systems (by CTR or two-color mechanisms). When generating a PDO with obliquely colliding laser pulses, the dipole length is determined by the angle of pulse collision and pulse duration, giving another control in generating PDO. From our simulations, at the optimum condition, we attained the energy conversion efficiency of PDO-THz up to 0.542×10^{-3}, with field strength ~ 9 GV/m. Any potential change of such a high efficiency due to 3D geometry, which we expect to be small, should be further investigated. As the limitation of angle-dependence in generating PDO have been removed by confirming that the obliquely colliding pulses can still generate the PDO very effectively, the efficiency can be enhanced further using much weaker but longer laser pulses with optimization of the pulse shape, as suggested in our previous research.[16]

AUTHOR DECLARATIONS

Conflict of Interest

The authors have no conflicts to disclose.

Author Contributions

Jaeho Lee: Data curation (lead); Investigation (equal); Writing – original draft (equal). **Hyung Seon Song:** Data curation (supporting). **Dohyun Park:** Data curation (supporting). **Manoj Kumar:** Data curation (supporting). **Bernhard Ersfeld:** Formal analysis (supporting); Writing – review & editing (supporting). **Samuel Yoffe:** Formal analysis (supporting); Writing – review & editing (supporting). **Dino Anthony Jaroszynski:** Writing – review & editing (supporting). **Min Sup Hur:** Formal analysis (equal); Software (equal); Supervision (equal); Validation (equal).

DATA AVAILABILITY

The data that support the findings of this study are available from the corresponding author upon reasonable request.

REFERENCES

[1] Q. Wu, T. D. Hewitt, and X.-C. Zhang, Appl. Phys. Lett. **69**, 1026 (1996).

[2] H. Cheon, J. H. Paik, M. Choi, H. J. Yang, and J. H. Son, Sci. Rep. **9**, 6413 (2019).

[3] Z. Zhang, A. S. Fisher, M. C. Hoffmann, B. Jacobson, P. S. Kirchmann, W.-S. Lee, A. Lindenberg, A. Marinelli, E. Nanni, R. Schoenlein *et al.*, J. Synchrotron Radiat. **27**, 890 (2020).

[4] H. Xu, L. Yan, Y. Du, W. Huang, Q. Tian, R. Li, Y. Liang, S. Gu, J. Shi, and C. Tang, Nat. Photonics **15**, 426 (2021).

[5] G. P. Gallerano and S. Biedron, in *Proceedings of the 2004 FEL Conference* (Comitato Conferenze Elettra, 2004), Vol. 1, p. 216.

[6] B. S. Williams, S. Kumar, Q. Hu, and J. L. Reno, Electron. Lett. **42**, 89 (2006).

[7] B. Zhang, Z. Ma, J. Ma, X. Wu, C. Ouyang, D. Kong, T. Hong, X. Wang, L. Chen *et al.*, Laser Photonics Rev. **15**, 2000295 (2021).

[8] J. Penano, P. Sprangle, B. Hafizi, D. Gordon, and P. Serafim, Phys. Rev. E **81**, 026407 (2010).

[9] U. Happek, A. J. Sievers, and E. B. Blum, Phys Rev. Lett. **67**, 2962 (1991).

[10] A. M. Cook, R. Tikhoplav, S. Y. Tochitsky, G. Travish, O. B. Williams, and J. B. Rosenzweig, Phys. Rev. Lett. **103**, 095003 (2009).

[11] Z. M. Sheng, K. Mima, J. Zhang, and H. Sanuki, Phys. Rev. Lett. **94**, 095003 (2005).

[12] U. Teubner, D. Altenbernd, P. Gibbon, E. Förster, A. Mysyrowicz, P. Audebert, J.-P. Geindre, J. C. Gauthier, R. Lichters, and J. Meyer-ter-Vehn, Opt. Commun. **144**, 217 (1997).

[13] I. V. Timofeev, E. A. Berendeev, V. V. Annenkov, E. P. Volchok, and V. I. Trunov, Phys. Plasmas **28**, 013103 (2021).

[14] E. Volchok, V. Annenkov, and I. Timofeev, Plasma Phys. Controlled Fusion **63**, 045001 (2021).

[15] A. Pukhov, A. Golovanov, and I. Kostyukov, Phys. Rev. Lett. **127**, 175001 (2021).

[16] K. B. Kwon, T. Kang, H. S. Song, Y. K. Kim, B. Ersfeld, D. A. Jaroszynski, and M. S. Hur, Sci. Rep. **8**, 145 (2018).

[17] R. Mankowsky, A. Subedi, M. Först, S. O. Mariager, M. Chollet, H. Lemke, J. S. Robinson, J. M. Glownia, M. P. Minitti, A. Frano *et al.*, Nature **516**, 71 (2014).

[18] M. Först, C. Manzoni, S. Kaiser, Y. Tomioka, Y.-N. Tokura, R. Merlin, and A. Cavalleri, Nat. Phys. **7**, 854 (2011).

[19] A. Dienst, M. C. Hoffmann, D. Fausti, J. C. Petersen, S. Pyon, T. Takayama, H. Takagi, and A. Cavalleri, Nat. Photonics **5**, 485 (2011).

[20] Z. Tibai, M. Unferdorben, S. Turnár, A. Sharma, J. Fülöp, G. Almási, and J. Hebling, J. Phys. B: At., Mol. Opt. Phys. **51**, 134004 (2018).

[21] E. A. Nanni, W. R. Huang, K.-H. Hong, K. Ravi, A. Fallahi, G. Moriena, R. Dwayne Miller, and F. X. Kärtner, Nat. Commun. **6**(1), 8486 (2015).

[22] Y. Socol, Opt. Laser Technol. **46**, 111 (2013).

[23] J. Pelka, K. Tybor, R. Nietubyc, and G. Wrochna, Acta Phys. Pol., A **117**, 427 (2010).

[24] J. M. Dawson, Phys. Rev. **113**, 383 (1959).

[25] M. Cho, Y. Kim, H. Suk, B. Ersfeld, D. A. Jaroszynski, and M. S. Hur, New J. Phys. **17**, 043045 (2015).

[26] Y.-K. Kim, M.-H. Cho, H. S. Song, T. Kang, H. J. Park, M. Y. Jung, and M. S. Hur, Phys. Rev. E **92**, 043102 (2015).

[27] Y.-K. Kim, T. Kang, M. Y. Jung, and M. S. Hur, Phys. Plasmas **24**, 073106 (2017).

[28] M. S. Hur and H. Suk, Phys. Plasmas **18**, 033102 (2011).

[29] M.-H. Cho, Y.-K. Kim, and M. S. Hur, Phys. Plasmas **20**, 093112 (2013).

[30] K. Yee, IEEE Trans. Antennas Propag. **14**, 302 (1966).

[31] J. Villasenor and O. Buneman, Comput. Phys. Commun. **69**, 306 (1992).

[32] J. P. Boris, in *Proceedings of Fourth Conference on the Numerical Simulation of Plasmas* (Naval Research Laboratory, 1970), pp. 3–67.

[33] S. Augst, D. D. Meyerhofer, D. Strickland, and S.-L. Chin, JOSA B **8**, 858 (1991).

[34] M. V. Ammosov, N. B. Delone, and V. P. Krainov, Sov. J. Exp. Theor. Phys. **64**, 1191 (1986); available at https://ui.adsabs.harvard.edu/abs/1986JETP...64.1191A/abstract.

[35] D. L. Bruhwiler, D. Dimitrov, J. R. Cary, E. Esarey, W. Leemans, and R. E. Giacone, Phys. Plasmas **10**, 2022 (2003).

[36] D. Bauer and P. Mulser, Phys. Rev. A **59**, 569 (1999).

[37] C. Tailliez, X. Davoine, A. Debayle, L. Gremillet, and L. Bergé, Phys. Rev. Lett. **128**, 174802 (2022).